Interpretation of Free Space Doors For Autonomous Visual Navigation

Jean-Yves Hervé
Computer Vision Laboratory
Center for Automation Research
University of Maryland
College Park, MD 20742
e-mail: herve@cfar.umd.edu

Abstract

This paper does not propose a new algorithm for path planning or obstacle avoidance, but a new type of visual information which can be exploited by such algorithms. Traditionally, a robot's visual system is assigned the task of reconstructing the geometry of the surrounding scene. The navigation problem can then be solved by means of classical robotics (control of mechanisms). Unfortunately, it is still impossible to accurately compute the depth maps robots are supposed to use for navigating. We propose here a new approach to the navigation problem, based on the exploitation of *free space doors*, and in which visual processes can be closely integrated with the control of the robotic system.

Résumé

Ce papier ne propose pas un nouvel algorithme pour la génération de trajectoire (ou de chemin) dans un environnement encombré d'obstacles, mais un nouveau type d'information visuelle qui peut être exploitée par de tels algorithmes. La tâche traditionnellement assignée au système visuel d'un robot autonome est la reconstruction de la géométrie de son environnement. Une fois ce problème résolu, la navigation autonome se reduirait alors à un problème de robotique classique (contrôle de mécanismes). Il est malheureusement toujours impossible de calculer le type de "cartes" sensées être utilisées par les algorithmes de navigation. Nous proposons dans ce papier une nouvelle approche au problème de la navigation, une approche basée sur l'exploitation de *portes d'espace libre*, et par laquelle les processus visuels peuvent être étroitement intégrés au contrôle du système robotique.

1 Introduction

We are interested in the problem of visual navigation, that is, of realizing autonomous robots able to perform complex *navigation* tasks in general terrestrial environments. This restriction essentially means that although the robot as well as all the objects in its environment are three-dimensional, it displacements are compliant to a locally two-dimensional surface (the horizontal plane in the case of an indoor environment, the local tangent plane in the case of terrain navigation). We can therefore reduce the obstacle representation and trajectory planning problems to the two-dimensional case.

The problem of trajectory planning (or, more often, path planning) for such a robot in a *known* environment has been the subject of many studies over the past decade. Currently, whether the goal of these work is an optimal solution or a heuristic one, there are two kinds of approaches to the motion planning problem: those who study simple robots (little or no dynamic constraints) in general 2D environments ([12], [9]), and those who study the control of complex (non-holonomic) robots in simple environments, generally with no obstacles ([1]).

On the other hand, there are now example of vision-guided mobile robots which are able to incorporate elements of both approaches and can avoid obstacles under dynamic trajectory constraints. Naturally, this can only be done at the cost of restricted environments and simpler models for the robots, but the most important lesson one can learn from the most successful of these robots is that efficient control is possible only if a good visual feedback is used: curvature of the road for autonomous road following ([5]) or structures found in an office environment in the case of indoor navigation ([4]).

The purpose of this paper is not the description of a particular path planning algorithm, but the presentation of a new type of visual feedback that can be used by existing algorithms for the control of autonomous navigation tasks. We present in Section 2 the concept of *free space doors* and show in Section 3 how this data can be exploited by motion planning algorithms.

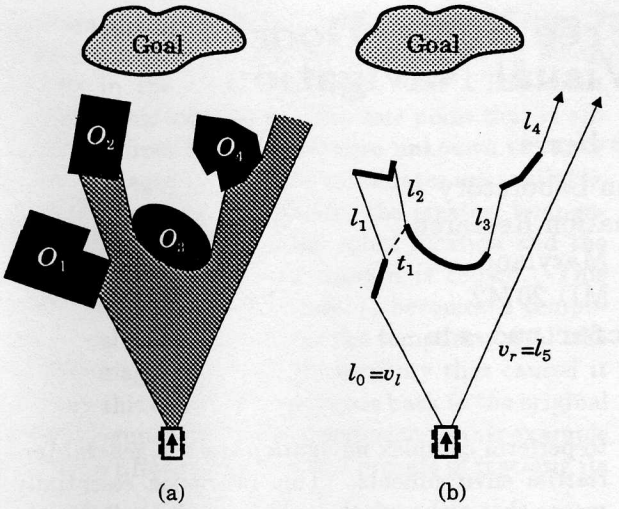

Figure 1 — The robot amidst obstacles and the free space doors

2 Visual Feedback for Navigation

2.1 Obstacles and Free Space Doors

Obstacle avoidance is hardly a task on its own; it will be performed during the realization of a more complex action: exploration, cleaning of an office environment, prey catching, etc. We will in consequence assume that the robot has knowledge of a *goal* it is trying to reach while attempting to dodge obstacles on its way. This goal could be a point of the workspace, or of the configuration space $\mathcal{S}$, but also an area of the workspace defined by the task at hand. For example, the robot may have to search for an object, or explore a given domain of its surroundings.

At every moment, the robot needs to know where it can go. In order to get this information, it does not *have* to determine the position, shape and motion of the obstacles it may find on its way: what really matters is where the *free space* lies. Because the robot does not possess complete information about its environment but must interpret that provided by its camera, it can at best detect the *apparent free space*.

Let us consider the 2-dimensional scene depicted in Figure 1(a). The robot is represented by the boxed arrow indicating the direction of motion, and the obstacles by the black blocks labeled O_1 through O_4. The robot's camera gives it information about the shaded area, which corresponds to the current apparent free space. From this particular position and orientation, the robot is unable to detect whether or not there is actually free space between O_1, O_2, O_3 and O_4, since all it can see of these obstacles is the dark lines drawn in Figure 1(b).

Rather than storing and updating the position and shape of these partial contours, we can notice that, in order to reach its goal, the robot has to cross either the lines limiting its field of view, v_l and v_r, or one of the longitudinal lines labeled l_i, for $i = 1, \ldots 4$, which correspond to occlusions in the scene. The problem of planning a path to the goal can therefore be redefined in terms of crossing such lines, which we consequently call *free space doors* ([8]). In some cases, the trajectory can be further constrained: before crossing l_1 or l_2 the robot would have to cross the transversal dashed line labeled t_1 first. Lines of l type (which includes v_l and v_r) will be called longitudinal doors, or l-doors, while t type lines will be called transversal doors or t-doors.

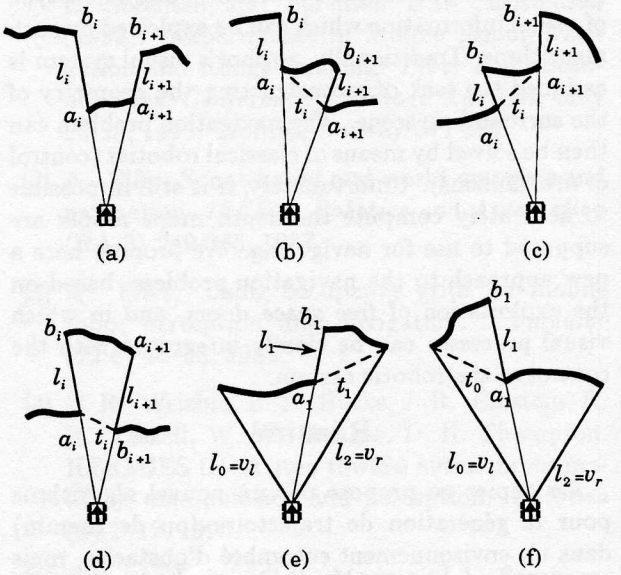

Figure 2 — Conditions for the existence of a transversal door

The existence and location of t-doors are entirely determined by the relative position of l-doors: scanning the robot's field of view from left to right, we number the l-doors as we encounter them, starting with $l_0 = v_l$ and ending with $l_n = v_r$, the left and right limits of the field of view respectively, and label each l_i either (+) or (−) according to the sign of the depth discontinuity. In Figure 2(b), l_1, l_3, and l_4 would be labeled (+), with l_2 the only (-). The endpoint of l_i closer to the robot is named a_i, the other one b_i, so that the door is represented by a 3-tuple: $l_i = (+, a_i, b_i)$ or $l_i = (-, a_i, b_i)$. Naturally, v_l and v_r are always (+) and (−) doors respectively, and a_l and a_r coincide with the optical center of the camera. If there exists a t-door t_i between l_i and l_{i+1}, its endpoints will be a_i and a_{i+1} and the robot

will cross t_i leaving a_i on its left.

Figure 2 summarizes the possible relative configurations of two l-doors that result in the existence of a t-door. More details on the properties of l-doors and t-doors, such as their orientation, can be found in [8]).

2.2 Corridors and Modifications of the Free Space Doors

The information provided by the free space doors at one particular instant is not sufficient to plan a collision-free, even if the non visible space should prove to be free. The reason for this is that, as was intended, free space doors do not completely represent the shape of obstacles. However, as the robot's position changes, so do the free space doors.

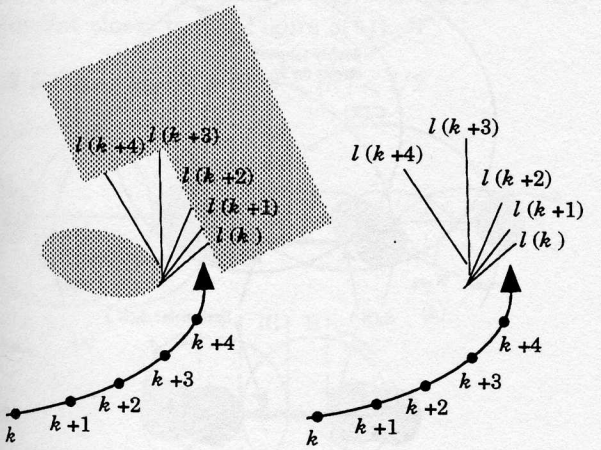

Figure 3 — A free space corridor

We notice in Figure 3 that the door undergoes modifications in position, orientation, and scale. The set of successive positions $\{l(kT),\ t \in \mathbb{N}\}$ defines the portion of free space currently under exploration; we call it a *free space corridor*[1]. In particular, as the robot encounters new corridors, and penetrates one of them in its attempt to reach the goal, it is in fact performing a depth first search on a graph of free space corridors which describes the free space available.

Free space doors can undergo more radical transformations as well: they can disappear (when the robot reaches a dead end) or split (generally when previously hidden free space between objects becomes visible). These modifications of individual doors can be interpreted to detect turns or exits to passageways ([7]), but the main value of doors remains as a data that can be best interpreted and exploited as a *dynamic* process rather than isolated snapshots.

[1] Our *corridors* should not be confused with the generalized cones used by [3] to decompose the free space in a *known* environment. The free space doors and corridors are dynamic, and extracted from the incomplete visual information available to the robot.

3 Planning a Path for the Robot

3.1 Free Space Doors and Configuration Space

In the free space door formalism, the path planning problem reduces to that of point obstacle avoidance, the obstacles being the endpoints of the doors the vehicle has to cross on its way to the goal. Let us model our robot as a cylindrical vehicle (Figure 4(a)) controlled by two variables: the tangential acceleration (deceleration) γ_t and the rate ω at which the steering parameter is changed, (generally, the angle velocity of the steering wheel). We can then reduces our robot to a point in the configuration space while growing the obstacles to the discs delimited by the circles $\mathcal{C}(L, r_0)$ and $\mathcal{C}(R, r_0)$ (Figure 4(b)).

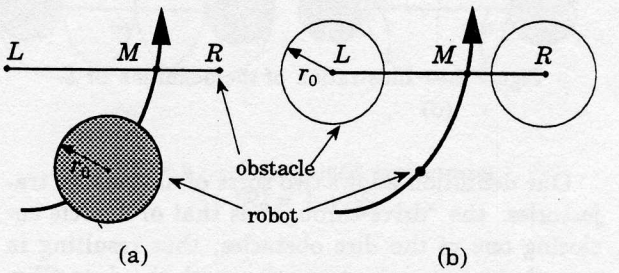

Figure 4 — (a) Intersecting a door (b) In configuration space

In addition, and *regardless of the shape of the obstacles in the 3D space*, we can now include to our planning dynamic constraints such as bounds on the velocity v, curvature κ, and acceleration (both on the tangential acceleration γ_t and on the normal acceleration $\gamma_n = \kappa \cdot v^2$).

3.2 Determination of the Intersection Space

3.2.1 Definition

Let a free space door be given, for which an orientation has been defined according to the results of Section 2. The intersection space $\mathcal{I}$ is defined as the set of *authorized intersection states*, that is, of vehicle configurations (M, φ, κ) such that there exists a circular trajectory of radius $\mathcal{R} = 1/\kappa$ intersecting the door at M with an angle φ, and which completely brings the robot from the front side of the door to the other, without colliding with the door's endpoints. Figure 5 gives examples of non authorized ((a) and (c)) and authorized trajectories ((b), (d), and (e)).

This definition would not be valid if our goal was to plan statically an optimal trajectory to the goal. In the case of our dynamic control, we can picture the planning problem as jumping every Δt from an authorized circular arc at $t = k\Delta t$ to an authorized arc at $(k+1)\Delta t$, by increments of the curvature $\Delta\kappa = \omega\,\Delta t$. Similar assumptions, on curvature and velocity have been made on systems which have proved remarkably successful in their restricted domain ([5]).

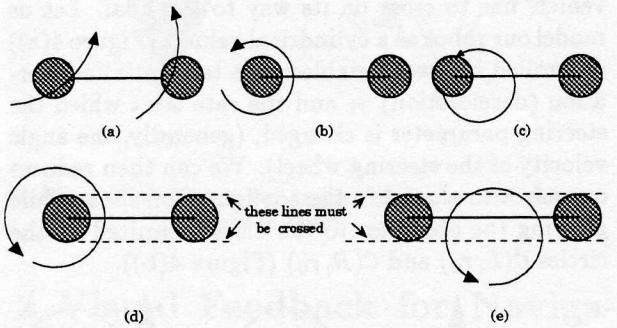

Figure 5 — Illustration of the definition of $\mathcal{I}$

Our definition allows two sorts of authorized trajectories: the "drive-through" is that of a circle enclosing one of the disc obstacles, thus resulting in a single transversal intersection with the door (Figure 5(d)). The "kiss-and-ride" type of trajectory only temporally leads the robot to the other side of the door, to bring it back to the same point (Figure 5(e)). For a more thourough justification of $\mathcal{I}$ and the need for "kiss-and-ride" trajectories, see [7].

3.2.2 Minimum and maximum authorized intersection angles

Let L and R be the left and right endpoints of the door to cross, of length $l = LR > 2r_0$. We consider a point M of the door of "door coordinate" $z = LM$, and we would like to calculate, for a given curvature κ (and the corresponding curvature radius $\mathcal{R} = 1/\kappa$), the values of the minimum and maximum angle, θ_m and θ_M, under which the vehicle can safely cross the door at M (see Figure 6). A look at the figure reveals that θ_m and θ_M correspond to trajectories tangent to the obstacles in configuration space, and that the problem is symmetric: $\theta_M(z,\mathcal{R}) = \pi - \theta_m(z,\mathcal{R})$. Another symmetry exists, with respect to the midpoint of the door, which results in the following relation: $\theta_m(z,\mathcal{R}) = \theta_m(l-z,-\mathcal{R})$.

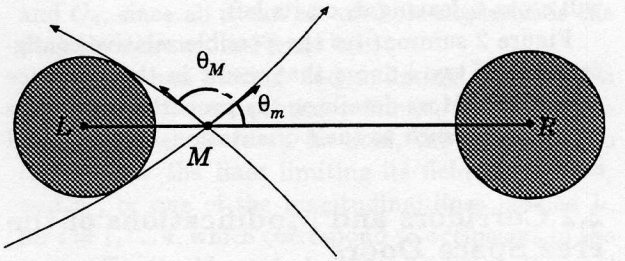

Figure 6 — Definition of θ_m and θ_M for curvature radius $\mathcal{R}$

We study now the evolution of θ_m for drive-through trajectories as $|\mathcal{R}|$ varies from ∞ to r_0. Subsection 3.3 will present a similar study for kiss-and-ride trajectories.

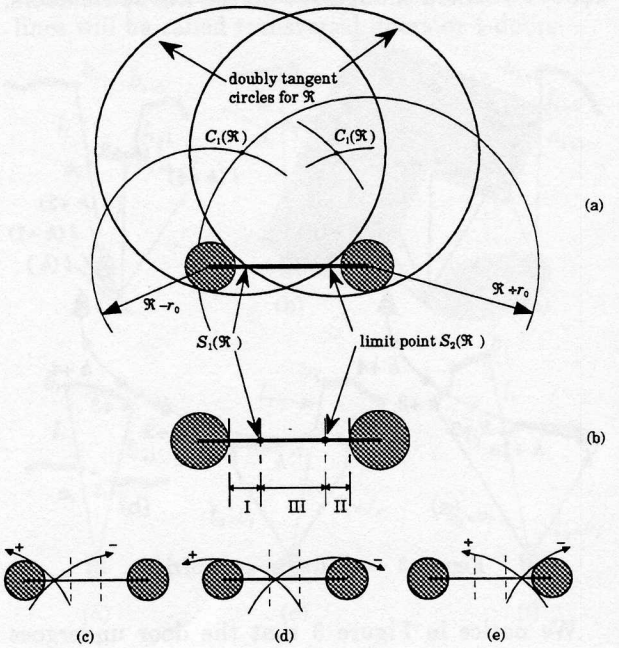

Figure 7 — Partition of the door: (a) the doubly tangent circles (b) the 3 parts

3.2.3 Case 1: $|\mathcal{R}| < l/2$

We can identify on the door two remarkable points, which we call $S_1(\mathcal{R})$ and $S_2(\mathcal{R})$, and for which there exist circular trajectories tangent to both obstacles (see Figure 7(a)). Let $z_1 = LS_1$ and $z_2 = LS_2 = l - z_1$ be the door coordinates of these points:

$$z_1 = \frac{l}{2} + \frac{2|\mathcal{R}|r_0}{l} - \frac{\sqrt{4r_0\,(2|\mathcal{R}| - r_0) + \left(\frac{4|\mathcal{R}|r_0}{l} - l\right)^2}}{2}$$

The free space door decomposes into three parts, as shown in Figure 7(b).

- **Case 1.a** If M belongs to part I, no circular path crossing the door at M can collide with R without

also colliding with L, the converse being not true: the path is only constrained by L, regardless of the sign of the curvature (Figure 7(c)).

- **Case 1.b** If M belongs to part II, the symmetric problem is encountered (Figure 7(e)).
- **Case 1.c** If M belongs to part III, the door's endpoint constraining the path is determined by the sign of the curvature, regardless of which half of the door M belongs to. The constraint point is L if $\kappa > 0$; it is R if $\kappa < 0$ (Figure 7(d))

3.2.4 Case 2: $|\mathcal{R}| = l/2$

S_1 and S_2 come in contact with the obstacle, thus giving only one doubly tangent circular trajectory instead of two for S_1 and S_2 ($C_1' = C_1$, $C_2' = C_2$ as in (Figure 8(a)). Whether the curvature is positive or negative, the path is only constrained by the endpoint closer to M (Figure 8(b)).

3.2.5 Case 3: $l/4 + r_0/2 < |\mathcal{R}| < l/2$

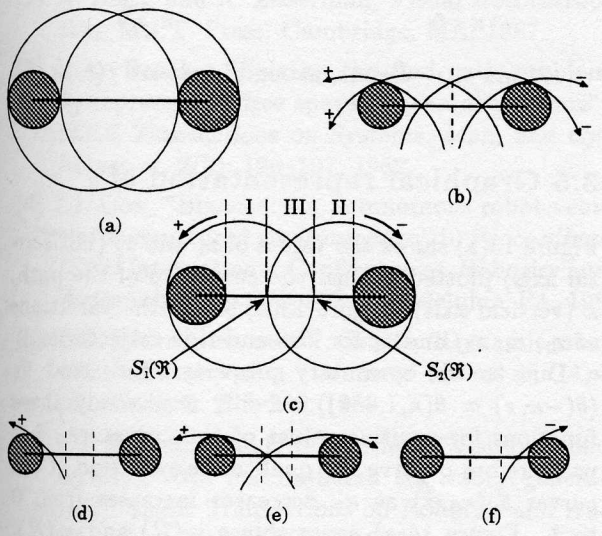

Figure 8 — Constrained trajectories:
(a): $|\mathcal{R}| = l/2$,
(c): $l/4 + r_0 < |\mathcal{R}| \leq l/2$

We can again distinguish two remarkable points, S_1 and S_2, which are the leftmost and the rightmost poinst on the door for which there is an authorized drive-through trajectory o radius $\mathcal{R}$ (Figure 8(c)). The door coordinates of S_1 and S_2 are $z_1 = l + r_0 - 2|\mathcal{R}|$ and $z_2 = 2|\mathcal{R}| - r_0$. These points partition the door in three parts, as in case 1.

- **Case 3.a** On part I, only trajectories of positive curvature are possible, and they are constrained by L (Figure 8(d))
- **Case 3.b** On part II, only trajectories of negative curvature are possible, and they are constrained by R (Figure 8(f)).
- **Case 3.c** On part III, trajectories of positive curvature are possible and constrained by L, while trajectories of negative curvature are constrained by R (Figure 8(e)).

3.2.6 Case 4: $|\mathcal{R}| = l/4 + r_0/2$

For $|\mathcal{R}| = l/4 + r_0/2$, segment $[S_1, S_2]$ collapses into a single point at the center of the door, on which it thus defines a bi-partition (Figure9(a)).

- **Case 4.a** On the left half, no drive-through trajectory with negative curvature is available, and positive curvature circular trajectories are only constrained by L (Figure9(b)).
- **Case 4.b** The situation is exactly symmetric on the other half of the door, the only authorized trajectories having negative curvature, and being constrained by R.

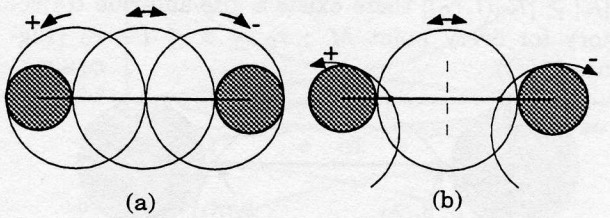

Figure 9 — Constrained trajectories:
$|\mathcal{R}| = \frac{l}{4} + \frac{r_0}{2}$

3.2.7 Case 5: $r_0 \leq |\mathcal{R}| < l/4 + r_0/2$

Once again, a segment forms around the door's midpoint, delimited by points $S_1(z1 = |\mathcal{R}| - r_0)$ and $S_2(z2 = l + r_0 - |\mathcal{R}|)$, so that it enlarges to converge to $[r_0, l - r_0]$ as $|\mathcal{R}|$ tends to r_0 (Figure'`extheta45`'(c)). The now familiar tri-partition of the door leads to the following interpretation:

- **Case 5.a** On part I, only trajectories of negative curvature, constrained by L are possible (Figure10(d)).
- **Case 5.b** The symmetric configuration occurs on Part II, and only paths of negative curvature, constrained by R are authorized.
- **Case 5.c** No drive-through trajectory is authorized on part III.

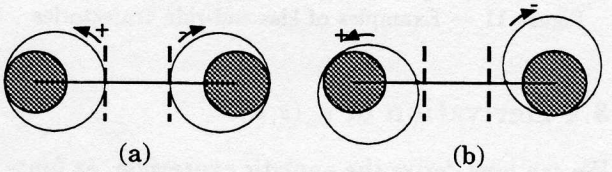

Figure 10 — Constrained trajectories:
$r_0 \leq |\mathcal{R}| \leq l/4 + r_0/2$

3.3 Authorized kiss-and-ride trajectories

The largest value of $|\mathcal{R}|$ for which a kiss-and-ride trajectory is defined is the one corresponding to the construction of Figure 11(a). A simple application of Pythagore's theorem give us $|\mathcal{R}_1| = 16l/r_0$.

As $|\mathcal{R}|$ decreases, we notice four remarkable points (see Figure 11(b)), S_3, S_4, S_5, S_6, of door coordinate

$$z_3 = \sqrt{4|\mathcal{R}|r_0} - \sqrt{r_0(2|\mathcal{R}| - r_0)}, \quad z_4 = l - z_3$$
$$z_6 = \sqrt{4|\mathcal{R}|r_0} + \sqrt{r_0(2|\mathcal{R}| - r_0)}, \quad z_5 = l - z_6$$

For all $|\mathcal{R}| \in [r_0, \mathcal{R}_1]$ and every door point $M(z)$, there exists no kiss-and-ride trajectory through M if and only if $z_5 < z < z_6$. In particular, if $l > 6r_0$, then for all $|\mathcal{R}| \geq |\mathcal{R}_2(l, r_0)|$ there exists a kiss-and-ride trajectory for every point $M : r_0 \leq z \leq l - r_0$ (Figure 11(c)).

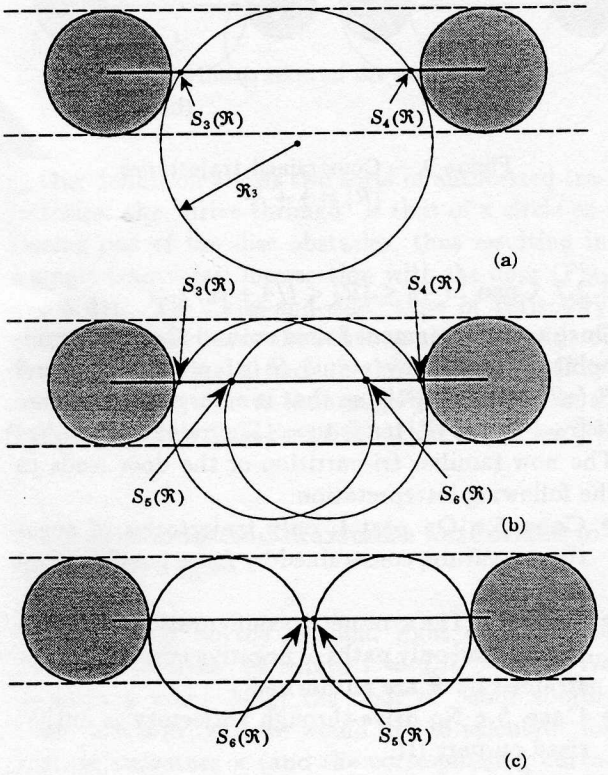

Figure 11 — Examples of kiss-and-ride trajectories

3.4 Derivation of $\theta_m(z, \kappa)$

We can now derive the analytic expression, as functions of κ and z of the smallest autorized intersection angle for a drive through trajectory, $f(z, \kappa)$ and for a kiss-and-ride trajectory, $g(z, \kappa)$. For example, Figure 12 shows how $f(z, \kappa)$ can be computed for a negative (a) and a positive curvature (b):

$$f(z, \kappa) = \sin^{-1}\left[\frac{r_0}{z} + \frac{|\kappa|(z^2 - r_0^2)}{2z}\right].$$

Similarly, for the kiss-and-ride trajectories, we obtain

$$g(z, \kappa) = \cos^{-1}(1 - |\kappa| \cdot r_0).$$

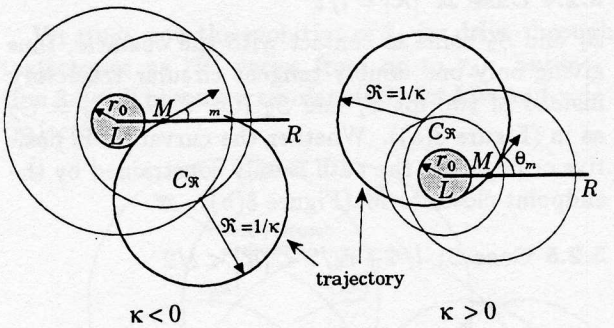

Figure 12 — Determination of function $f(z, \kappa)$

3.5 Graphical representation of $\mathcal{I}$

Figure 13(a) shows the values of z_1 and z_2 (horizontal axis) plotted against the curvature of the path, κ (vertical axis). Figure 13(b) shows the variations of z_3, z_4, z_5, and z_6 for kiss-and-ride trajectories.

Due to the symmetry property of θ_d and θ_k ($\theta(-\kappa, z) = \theta(\kappa, l - z)$) we only need study these functions for positive values of the curvature. Let us therefore observe the qualitative evolution of the curves $\theta_d(\kappa_0, z)$ as κ_0 decreases increases from 0 to 1. Figure 14(a) again shows $z_1(\mathcal{R})$ and $z_2(\mathcal{R})$, and decomposes interval $[0, 1]$ into seven segments or points.

For $\kappa = 0$, the trajectory is a straight line. We know from Figure 14(a) that $z_1(\mathcal{R})$ and $z_2(\mathcal{R})$ coincide with the door's midpoint, and we observe in Figure 14(b) a corner point at this location, where the two half curves meet (one being constrained by the left endpoint, the other by the right endpoint, as was explained earlier). As κ decreases, the corner moves toward the right endpoint of the door (Figure 14(c)) and reaches it (vanishes) for $\kappa = 1/\mathcal{R}_1 = 2/l$ (Figure 14(d)). Further decreasing κ results in reducing the domain $[r_0, z_2(\mathcal{R})]$ of the function (Figure 14(e)) until $\kappa = 1$, for which the curve is reduced to an isolated point (Figure 14(h)). Interestingly, whether κ is larger than $1/\mathcal{R}_2 = (\frac{l}{4} + \frac{r_0}{2})^{-1}$ (Figure 14(e)) or not (Figure 14(g)) has no significant effect on the shape of the curve.

4 Conclusion

We have presented the concepts of free space doors and corridors, a new type of dynamic feedback for autonomous visual navigation. We have shown that this information could be exploited by classical planning techniques to control the trajectory of an autonomous robot in obstacles avoidance tasks. Finally, we completed our presentation by deriving the configuration space constraints associated one free space door, and exposing the elements of our general navigation system.

References

[1] B. d'Andréa-Novel, G. Bastin, and G. Campion, "Modeling and control of non holonomic wheeled mobile robots," in *Proceedings IEEE International Conference on Robotics and Automation*, pp. 1130–1135, Sacramento, CA, 1991.

[2] A. Blake and A. Zisserman, *Visual Reconstruction*, M.I.T. Press, Cambridge, MA, 1987.

[3] R.A. Brooks, "Solving the find-path problem by representing free space as generalized cone", *IEEE Transactions on Systems, Man, and Cybernetics*, **2**(2): 190–197, 1982.

[4] I.J. Cox, "Blanche: An autonomous robot vehicle for structured environments," in *Proceedings IEEE International Conference on Robotics and Automation*, pp. 978–982, Philadelphia, PA, 1988.

[5] E.D. Dickmanns and W. Graefe, "Dynamic monocular machine vision," *Machine Vision and Applications*, **2**: 223–240, 1988.

[6] J.T. Feddema and O.R. Mitchell, "Vision-guided servoing with feature-based trajectory generation," *IEEE Transactions on Robotics and Automation*, **2**(5): 691–700, 1989.

[7] J-Y Hervé, "Navigational Vision," Ph.D. Thesis, Computer Science Department, University of Maryland, College Park, MD, 1993.

[8] J-Y Hervé, "Dynamic interpretation of free-space doors for visual navigation CAR-TR-581, Center for Automation Research, University of Maryland, College Park, MD, 1991.

[9] O. Khatib, "Real-time obstacle avoidance for manipulators and mobile robots," *International Journal of Robotics Research*, **2**(1): 90–99, 1986.

[10] D. Raviv and M. Herman, "Visual control signals for road following," in *Proceedings IEEE International Symposium on Intelligent Control*, pp. 436–442, Arlington, VA, 1991.

[11] C.K. Yap, "How to move a chair through a door," in *Proceedings IEEE International Conference on Robotics and Automation*, pp. 1320–1325, Raleigh, NC, 1987.

[12] C.K. Yap, "Algorithmic motion planning," in *Advances in Robotics. Volume 1: Algorithmic and geometric aspects*, J.T. Schwartz and C.K. Yap, editors, Lawrence Erlbaum Associates, Hillsdale, NJ, 1986.

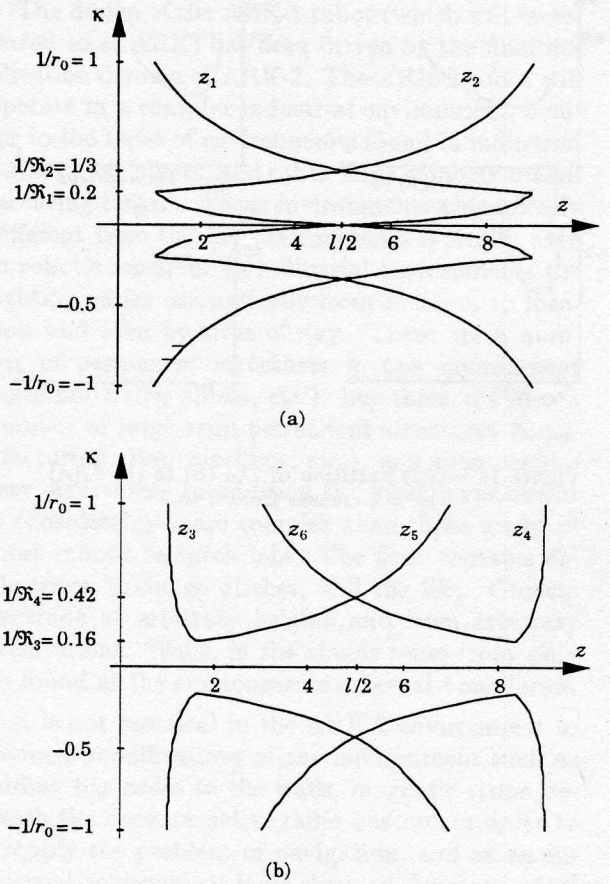

Figure 13 — $z_1, z_2, z_3, z_4, z_5, z_6$ plotted horizontally against the curvature

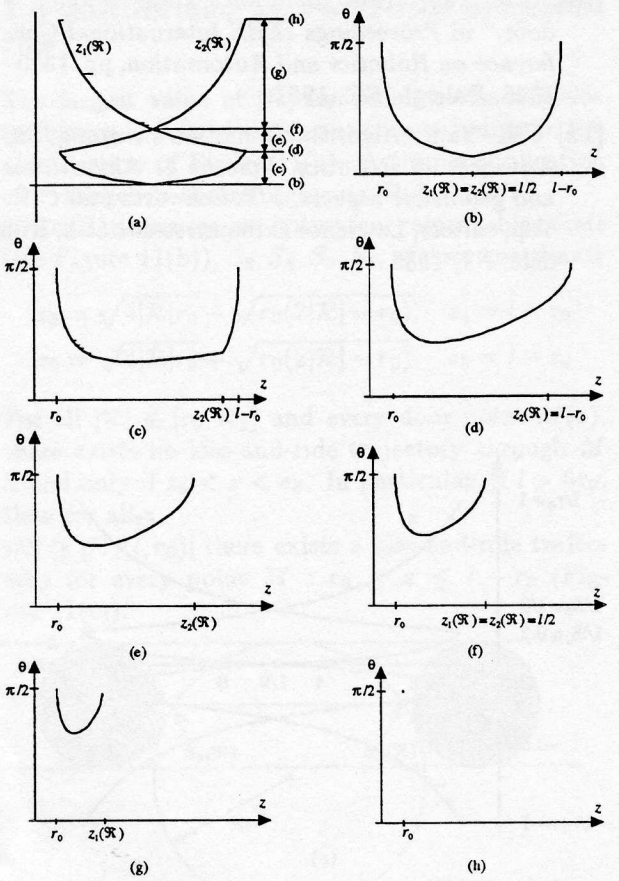

Figure 14 — (a) Partition of $\mathcal{D}_d$; (b) to (h) $\theta_d(\kappa)$ as κ increases from 0 to 1